Electrospun PVDF with Novel Facile Synthesized Functionalized Boron Nitride Quantum Dots for Neural Applications

Basma Ekram[1*], Ryan P. Trueman[2,3], James B. Phillips[2,3], Helena Ros[2,3], Bothaina M. Abdel-Hady[1], Dalia M. El-Gendy[4*]

[1]Polymers and Pigments Department, Chemical Industries Research Institute, National Research Centre, Dokki, 12622, Cairo, Egypt.
[2]Center for Nerve Engineering, UCL, London, United Kingdom.
[3]Department of Pharmacology, UCL School of Pharmacy, University College London, 29-39 Brunswick Square, London, United Kingdom. WC1N 1AX.
[4]Physical Chemistry Department, Advanced Materials Technology and Mineral Resources Research Institute, National Research Centre, Dokki, 12622, Cairo, Egypt.

*Corresponding author emails: Basma Ekram: basmaekram@yahoo.com
Dalia M. El-Gendy: dalia_elgendy2015@aucegypt.edu

Graphical Abstract

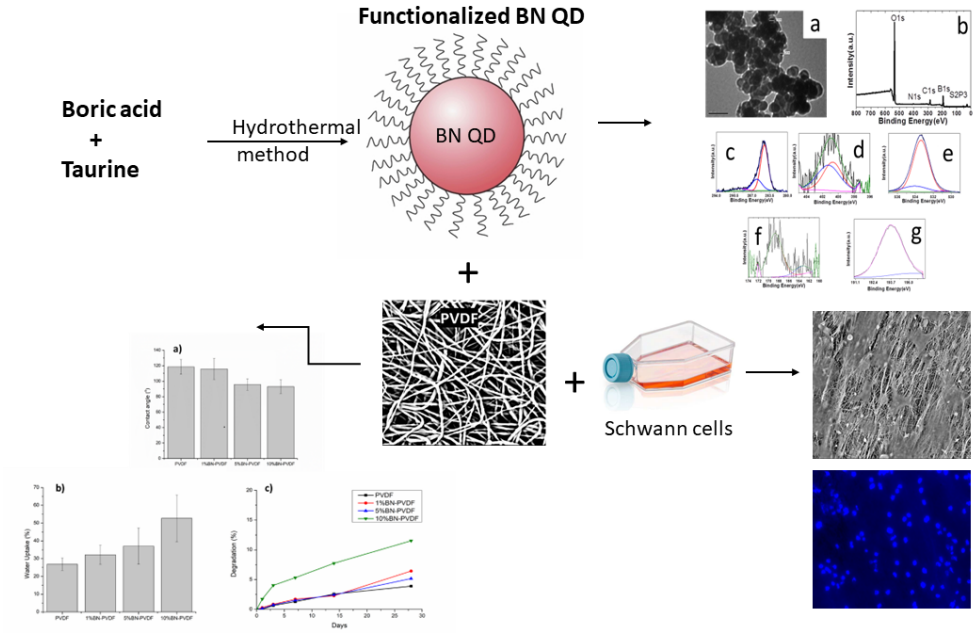

Abstract

The study aimed to develop a potential biomaterial for neuroregeneration by the electrospinning of the biocompatible polymer Polyvinylidene Fluoride (PVDF) with innovative functionalized boron nitride quantum dots (F-BNQDs) synthesized via green chemistry using the amino acid taurine as a functionalization. The F-BNQDs were characterized and were found to be 16–21 nm in diameter, showed good photoluminescent characteristics, and their elemental composition was confirmed by XPS, FTIR and UV. The

PVDF with F-BNQDs was prepared at three different concentrations, and the resulting electrospun fibres were characterized by SEM, FTIR, TGA, contact angle, biodegradation, water uptake, Schwann cell cytotoxicity, and cell behaviour studies. The results of the study showed that the addition of F-BNQDs to PVDF resulted in enhanced mechanical properties, decreased contact angle, increased degradability, and water uptake. The LDH assay revealed that 5% BN-PVDF had the lowest cytotoxicity. DAPI staining showed that the increase in F-BNQD concentration up to 5% BN-PVDF enhanced cell behaviour on the electrospun fibres. Therefore, the study concluded that 5% BN-PVDF would be suitable for further testing as a potential biomaterial for neuroregeneration *in vivo*.

Highlights

- Functionalized boron nitride quantum dots were prepared using amino acid Taurine.
- The F-BNQDs were characterized and electrospun with PVDF.
- The incorporation of F-BNQDs to PVDF has enhanced its physicochemical properties.
- All samples showed a single β phase PVDF.
- Schwann cells showed excellent compatibility and cell adhesion on F-BNQDs/PVDF.

Keywords: Functionalized boron nitride quantum dots, Electrospinning, PVDF, Taurine, Schwann cells

Introduction

Peripheral nerve injuries have the potential to cause total transection of the nerve, necessitating surgical intervention to enable the regrowth of axons from the injured site to the respective target organs [1]. In cases where the gap between the severed ends is too large, direct surgical repair is not feasible, and alternative approaches such as bridging the gap are required [2]. Currently, the most widely accepted treatment for such injuries is the use of nerve autografts, which involves taking a nerve from the same individual, but from a less critical location [3].

An alternative source of viable structures to bridge this gap and facilitate nerve repair is the use of electrospun conduits fabricated from synthetic and biological polymers [4–6]. Synthetic polymers like polycaprolactone, polylactic glycolic acid with and without dopants are used intensively in fabricating electrospun nerve conduits due to their fiber forming ability

[7, 8] as well as the usage of Polyvinylidene fluoride and Poly-vinylidene fluoride–trifluoroethylene [9–12].

These electrospun conduits can possess therapeutically beneficial nanofibrous morphology with high porous structure and high surface area to volume ratio, soft, tissue like mechanical characteristics and biocompatibility with the peripheral nervous system [13–17].

Recently, the need for smart nerve grafting materials has been growing, as these materials can react to different stimuli such as chemical, physical, or mechanical features and produce a response locally. An example of this would be piezoelectric materials [18]. Many electrospun piezoelectric materials have been studied and they have reported high biocompatibility[19].

Polyvinylidene fluoride (PVDF) is a piezoelectric polymeric material that has gained significant attention in recent years within regenerative medicine [20–22], including within peripheral nerve repair [11, 23]. The piezoelectric characteristics of PVDF allow it to transform mechanical energy into electrical energy [24, 25], enabling it to deliver localized electrical stimulation to cells, leading to increased migration in a wound healing context [26, 27]. Furthermore, cells of the nervous system can respond positively to electrical stimulation [28], and the use of piezoelectric materials may provide electrical stimulation of a large enough magnitude to be therapeutically relevant [29]. Electrospun PVDF fibres are exciting as a novel biocompatible polymer for neuroregeneration applications due to their processability, scalability and the controlled morphology enabled by electrospinning, and their unique piezoelectric properties [20, 30]. Electrospinning also presents the opportunity to add additional therapeutic molecules to the final material [31]. Electrospun PVDF exhibits five molecular chain arrangements which are α, δ, β, γ and ε phases. Three of them are polar (δ, β, γ) and the β phase has the highest piezoelectric property [32, 33].

Different materials have been introduced to PVDF to enhance its properties such as other polymers, nanomaterials and nanotubes [19]. Cheng and his coworkers blended PVDF with Polycaprolactone to enhance its mechanical properties and nerve forming ability[34]. Also Gryshkov and his coworkers used trifluoroethylene (P(VDF-TrFE)) with PVDF to enhance its biocompatibility leading to a higher neurite growth. Ge et al used gold nanoparticles as a curcumin drug carrier with PVDF for drug delivery into neural tissues[35]. Abzan et al used graphene oxide nanoparticles incooperated with PVDF to enhance mechanical properties and cellular viability[36].

Boron Nitride (BN) is an example of a biocompatible piezoelectric material that can be used in the form of quantum dots [37, 38]. It has high chemical stability, and it was reported to improve the viability and proliferation of osteoblasts and also improve the mechanical properties when added to different polymeric scaffolds [39, 40]. Moreover, it is reported that BN functionalized scaffolds helped in microvessel regrowth and could stop the atrophy of muscles after denervation in a sciatic nerve injury model of the rats [40]. Quantum dots (QDs) are advanced fluorescent nanoparticles that have a diameter of approximately 20 nm or less that represent high surface area to volume ratio with unique properties compared to conventional materials [41]. Researchers studied the incorporation of quantum dots with PVDF but no studies up to our knowledge were done on nerve regeneration nor investigated the incorporation of boron nitride quantum dots with PVDF[42].

Taurine is a semi-essential sulfur-containing amino acid which is produced mainly by the liver and kidney [43] and has been linked with an important role in neurological disorders such as Alzheimer's, Huntington's and Parkinson's diseases [43–45]. It is also reported to protect against sciatic nerve myelin damage in a rat model of peripheral neuropathy [46], and to promote proliferation and promote neurogenesis of neural stem/progenitor cells in culture [47].

In this experimental report, novel functionalized piezoelectric boron nitride in the form of quantum dots were synthesized by taurine via the hydrothermal method to enhance the properties of non-functionalized BNQDs. The prepared quantum dots were electrospun with the biocompatible PVDF to increase the conductivity of material and alter the surface properties of the electrospun PVDF fibres to enhance the neurocompatibilty of the resultant nanofibers. The resultant electrospun mats made using 3 different concentrations of the functionalized boron nitride quantum dots were investigated and characterised.

2. Experimental

2.1. Materials

Polyvinylidene Fluoride (PVDF), Taurine and Boric acid were purchased from Alfa Aeser (Germany). Acetone (HPLC grade) was purchased from Sigma Aldrich. Dimethyl formamide (DMF) was acquired from Edwic (Egypt).

2.2. Preparation of functionalized boron nitride quantum dots (F-BNQDs)

Functionalized boron nitride quantum dots (F-BNQDs) were prepared by a single pot novel method via a hydrothermal process [48]. 0.1 g of boric acid with 0.0339 g of taurine were added to 10 mL of MilliQ water. The resulting mixture was then left in a Teflon-lined stainless-steel autoclave at 170 °C for 48 h. The resultant solution was frozen at -80 °C for 48 h and then subjected to lyophilization.

2.3. Electrospinning of PVDF loaded with F-BNQDs

Polymeric solution of 12% PVDF was prepared by dissolution in DMF and after complete dissolution of PVDF, acetone was added, with a final solvent ratio of 60:40 DMF:acetone as it was the optimum solvent ratio to produce β phase electrospun PVDF[49]. For F-BNQDs loaded samples, F-BNQDs was added to DMF and subjected to ultrasonication for 1h in order to prepare three concentrations (1, 5 and 10% wt/wt), then PVDF was added as described. The polymeric solutions were inserted into a syringe with a 20G needle and the tip to collector distance was set as 16 cm then 20 kV was applied by a Glassman High Voltage Series. For residual solvent removal after electrospinning, the electrospun fibre samples were vacuum-dried at 40°C for 3 h.

2.3 Physiochemical Characterizations

The morphology of the quantum dots was studied by a high resolution transmission electron microscope (Jeol/JEM-2100) operating at an acceleration voltage of 120 kV. UV/Vis spectrophotometry was performed with a Shimadzu 2040 spectrophotometer, while the photoluminescence spectra (PL) were attained using a fluorescence spectrometer (ThermoScientific LUMINA). The elemental composition of the quantum dots was determined using X-ray photoelectron spectroscopy (XPS, Thermo-Scientific ESCALAB/250Xi X-ray). The viscosity of the prepared solutions was studied using a Brookfield viscometer (DV-III Ultra) under uniform temperature of 25^{o}C via a S21 spindle rotating at 50 RPM. The conductivity change after the addition of F-BNQDs to PVDF polymeric solution was determined by using a conductivity meter (HC3010/Trans instruments) at 25 ^{o}C. Fibre diameter and morphology were studied using a field emission Scanning Electron Microscope (SEM, Jeol/JXA840) with attached EDAX. Mean fibre diameter of the samples was obtained by

determining about 50 different fibre lengths via ImageJ 1.42q software [50]. Fourier-transformed infrared (FTIR) spectroscopy was conducted using an attenuated total reflectance-FTIR spectroscope (Agilent). To analyze the surface hydrophilicity, the contact angle of five different material samples was measured using a horizontal camera that was perpendicular to the plane of the liquid droplet and the data analyzed using ImageJ software [50]. The samples were subjected to thermogravimetric analysis (TGA) using an SDTQ600 analyzer under argon at a rate of 10 °C per minute. The tensile strength of nanofibres with dimensions of 10 mm ×80 mm with a gap length of 20 mm, was tested using a Universal Testing Machine (Lloyd Instruments/LR10 K) at a stroke rate of 2 mm per minute. Each sample was tested four times and the results were averaged.

2.4 *In vitro* study

2.4.1 Degradation and water uptake

Three different mats from the same sample were cut into 2×1 cm^2 pieces and then weighed to determine initial weight (W_i). Then, the samples were incubated at 37°C for 1, 3, 7, 14 and 28 days in a Phosphate Buffered Saline (PBS). After each specified time point, the samples were taken out the PBS and slightly dried from the adsorbed saline on the material surface, then the samples were weighed to determine the wet weight (W_w). The samples were dried for 2 h in a vacuum oven and weighed again after drying to establish the dry weight (W_d). The weight loss and the water uptake percentages were determined by the following equations (Deyab et al. 2022):

$$\text{Weight loss } (\%) = \frac{W_i - W_d}{W_i} \text{ x } 100 \quad (1)$$

$$\text{Water uptake } (\%) = \frac{W_w - W_i}{W_i} \text{ x } 100 \quad (2)$$

2.4.2 Cell culture

The SCL4.1/F7 rat Schwann cell line, obtained from the Health Protection Agency, was grown in Dulbecco's Modified Eagle Medium (DMEM-Gibco). The media was supplemented with streptomycin 100 mg ml^{-1} and penicillin 100 U ml^{-1} (Sigma-Aldrich) and 10% fetal bovine serum (Thermo Fisher scientific). The cultures were proliferarted in a humidified 37 °C incubator with 5% CO_2, and the media was replaced every two to three days. The cells were harvested at the sub-confluent level (roughly 60-70% confluency).

2.4.3 Seeding Schwann cells on electrospun piezoelectric fibres

SCL4.1/F7 Schwann cells (10,000 per fibre) were seeded onto the top surface of 1 cm diameter cut circles of electrospun piezoelectric fibres The fibres were placed in the bottom of a 24 well plate (Thermo Fischer Scientific, UK) and stainless-steel washers (IKEA, Sweden) were placed on top of the fibres, creating a small well with just less than 1 cm diameter. Next, 50 μL of media including 10,000 cells was seeded on the top of the fibres and left to settle for 30 minutes. After 30 minutes incubation, the wells were gently filled to a final volume of 1 mL of media. The cells were allowed to adhere and grow on the fibres until further analysis.

2.4.4 Cell cytotoxicity and viability in response to electrospun fibres

Cell cytotoxicity was evaluated using a Lactate Dehydrogenase (LDH) assay carried out following the manufacturer's protocol (Abcam, UK). It was performed at 24 and 48 h post cell seeding on fibres. Absorbance from the assay was read at 450 and 650 nm. To evaluate cell growth on the electrospun fibres, DAPI was utilized to stain the nuclei of cells. Cells were then counted using a Zeiss AxioLab fluorescence microscope, with 3 fields of view captured from 3 independent fibre mats.

2.4.5 Scanning Electron Microscopy of SCL1.4/F7 Schwann Cells seeded on piezoelectric fibres

Cell morphology and attachment to different piezoelectric fibres were evaluated qualitatively using Scanning Electron Microscopy (SEM). Cells were grown on the fibre disks for 1 week before fixing in 4% PFA at 4°C overnight. Afterwards, the fixed samples were subjected to dehydration through a series of ethanol washes of increasing concentrations, starting with 5 minutes in both 50% and 75% ethanol, and then 30 minutes in 80%, 90% and 100% ethanol. Samples were taken out and then attached to a carbon SEM stub (Taab, UK), soaked in hexadimethylsilane and dried in a fume cupboard overnight. A Phenom Pro benchtop SEM was used to capture images of the electrospun fibres after sputter coating with gold.

2.4.6 Statistical analysis of cellular assays

To determine the viability and proliferation of Schwann cells when seeded to the samples, a Shapiro-Wilk test was conducted. One-way or Two-way ANOVA were then used

with post hoc tests where appropriate, as described in the relevant figure legends (GraphPad Prism 9.0.0). Data are represented as a mean ± standard error.

3 Results

3.1 Characterization of quantum dots

TEM was used to study the size and morphology of the functionalized BNQDs. In **Fig. 1(a),** The particles exhibit a spherical morphology with an average diameter ranging from approximately 16 to 21 nm. To confirm the F-BNQDs formation, the elemental composition was examined by XPS and displayed in **Fig. 1(b)**, which shows five peaks corresponding to C1s, an O1s, a B1s, an N1s, and an S2p, with resultant atomic percentages of 14.03, 77.35, 7.38, 0.8, and 0.43%, individually. The C1s high-resolution spectra are shown in **Fig. 1(c)**, with peaks at 284.5 eV assigned primarily to the C-C and B-C bonds, 286.05 attributed to the C-C/C=C, C-N, and 289.46 bonds related to C-N/C-O-B bonds [53, 54].

The peaks related to the bond components were assigned to the amino and amide groups. These findings suggest that taurine has effectively functionalized boric acid. The B1s 3d are shown in **Fig. 1(d)**, indicating the presence of one with peaks at 193.67 B-C [55]. The N1s spectrum was deconvoluted to examine the properties of nitrogen species, as presented. In **Fig. 1(e)**, two peaks at 401.24 eV and 400.7 eV could be assigned to the C-N bonding and amine/amide groups, sequentially, per the FTIR spectra [56]. For the O1s spectrum, **Fig. 1(f)**, the peak at 531.05.7 eV is according to the S=O bond, while the peaks at 533.9 eV and 534.06 eV reveal the C-OH bond. **Fig. 1(g)** reveals the existence of peaks related to S2p at 168.7 eV, indicating surface adsorbed oxidised sulphur species[57, 58]. The S2p spectrum shows peaks at 163.45 eV, which correspond to thiopene owing to the way S attaches to boron and quantifies the presence of sulphur.

The FTIR spectrum of the functionalized boron nitride quantum dots is displayed in **Figure 2(a)**. The absorption band centred at 3179 cm^{-1} is assigned to the stretching vibrations of N-H and O-H [59]. The peak at 1415 cm^{-1} is assigned to the C–N stretching vibration. The B-C absorption peak appeared at around 1192 cm^{-1}. The band at 1605 cm^{-1} is for C-N. The peak at 1032 cm^{-1} can imply the stretching vibration of the C-O bond.

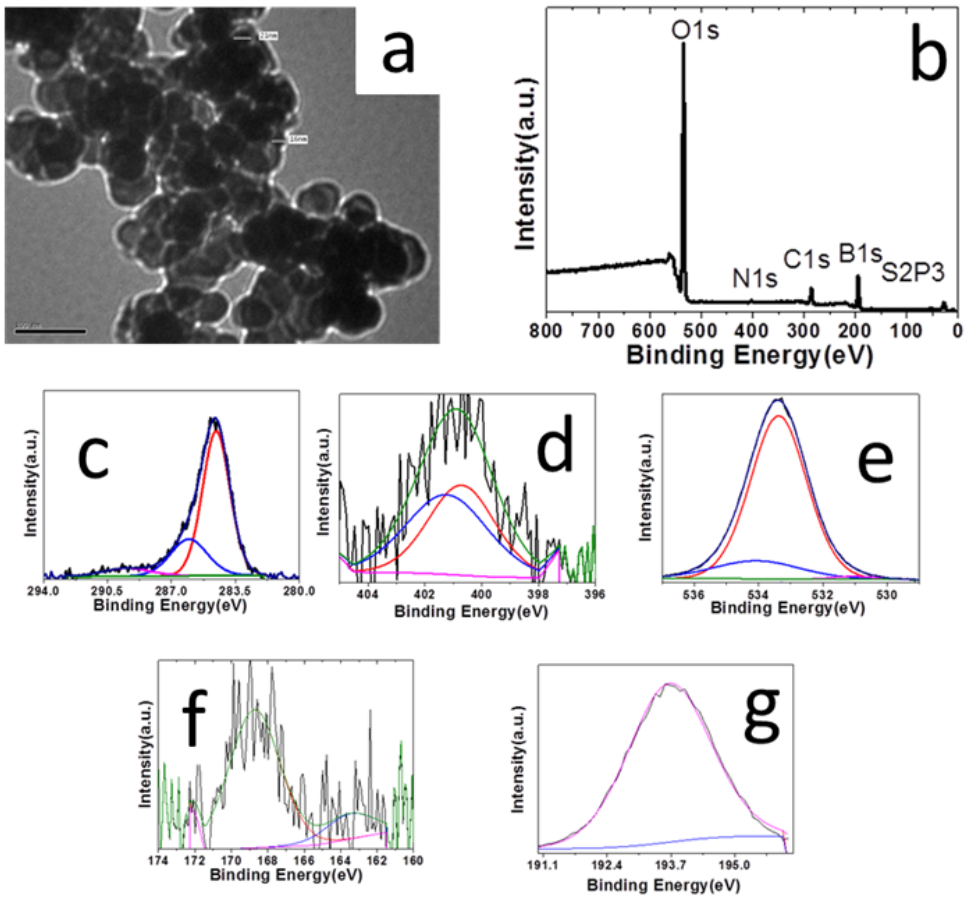

Figure 1: (a) TEM images of the F-BNQDs, XPS analysis: (b) survey, and high resolution (c) C1s, (d) N1s, (e) O1s, (f) S, and (g) B spectra of the F-BNQDs.

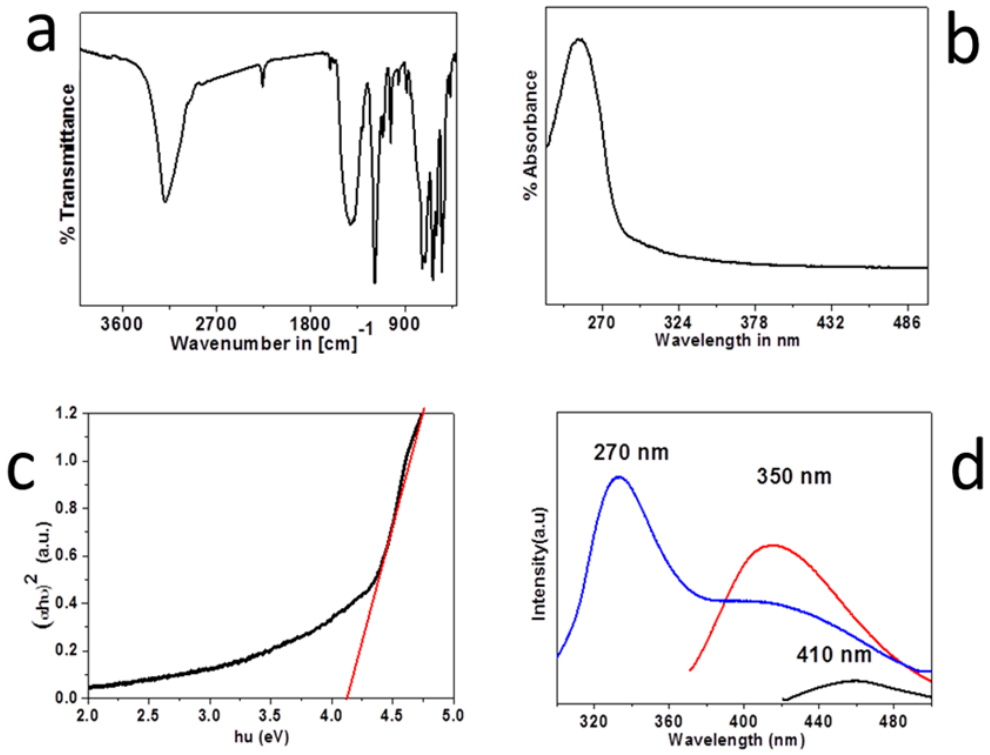

Figure 2: (a) FTIR (b) UV absorption, (c) band gaps and (d) PL spectra of the F-BNQDs excited at different wavelengths.

The band at 2259 cm^{-1} may indicate a stretching vibration of the C-H bond. The peak at 636 cm^{-1} may signify the existence of C-O and C-H bonds, respectively, while peaks at approximately 533 cm^{-1} could be attributed to the presence of O-H bonds. The vibrational peaks found around 1307 and 866.5 cm^{-1} assigned to the B-N stretching and bending modes, respectively [38, 60–62]. **Figures 2(b) and (c)** display the optical absorption spectrum with the Tauc plot for the F-BNQDs); the sample showed a typical UV absorption peak at 255 nm (F-BNQDs), and the energy band gap of (F-BNQDs calculated by the Tauc plot was Eg = 4.1 eV [63]. **Figure 2(d)** depicts the F-BNQDs illuminated by a UV lamp with a wavelength of 365 nm. The PL spectra of F-BNQDs can be observed at various excitation wavelengths such as 270, 350, and 410 nm of ultraviolet (UV) light. The optimal emissions were noticed at a wavelength of 400 nm, as depicted in **Figure 2(d)**. The fluorescence of F-BNQDs depends on the excitation source [64]. This can be attributed to various factors such as the existence of functional groups, trap states, and inhomogeneous chemical structure on the surface of the F-BNQDs [65]. The primary source of fluorescence emission arises from both emissive traps and different functional groups. The dependence of the emission on excitation is attributed to certain emissive sites being excited at a specific wavelength. Additionally, the discrete nature

of the distribution of phonons in the nanostructures and the quantum confinement besides the size effect contribute to the excitation-dependent behaviour of F-BNQDs. The size of quantum dots is inversely related to their energy band gap, as a result the smaller quantum dots have a larger energy band gap. The non-uniform distribution of F-BNQDs causes energy gap deviations, resulting in a broad emission wavelength that covers nearly the entire visible region. The PL properties of (F-BNQDs) indicate that they can be used in a variety of fields due to their excellent fluorescent performance [66, 67].

3.2 Characterisation of PVDF with F-BNQDs

Viscosity and Conductivity of the polymeric solutions was tabulated in **Table 1**. As shown the viscosity increases as the F-BNQDs concentration increases, which indicates the interaction of the F-BNQDs with the polymeric chains of PVDF. The conductivity measurements indicated that conductivity increases with increasing quantum dot concentration, presumably due to the semi-conductive nature of BNQDs which enhances the polymeric solution conductivity.

Morphology of the nanofibers was examined to study the impact of increasing F-BNQDs concentration on the morophological structure of the PVDF nanofibers. As presented in **Fig. 3**, all the samples are in the nano-range with smooth structure. The PVDF showed the largest fibre diameter (300 ±97 nm) and by increasing the F-BNQDs concentration the fibre diameter decreases to become 163±81 nm in case of 10% BN-PVDF. This decrease may be ascribed to the interaction between the F-BNQDs and the polymeric chains of PVDF that lead to the increase in viscosity which resulted in decreased fibre diameter. The results is consistent with the results obtained by Xue and Hu in their study of the impact of BN on silk nanofibers [68]. The EDAX analyses showed the incorporation of the F-BNQDs into the nanofibers of PVDF as presented in **Fig. 4**. As the concentration increases the peak of the boron and nitrogen increases.

Table 1: The viscosity and conductivity of polymeric solutions of PVDF and PVDF with F-BNQDs.

Sample name	Viscosity (cP)	Conductivity (µS)
PVDF	249±5.6	12.4±1.3
1% BN-PVDF	254±2.9	19.9±3.9
5% BN-PVDF	285±8.6	32.6±5.8
10% BN-PVDF	301±3.4	53.8±7.8

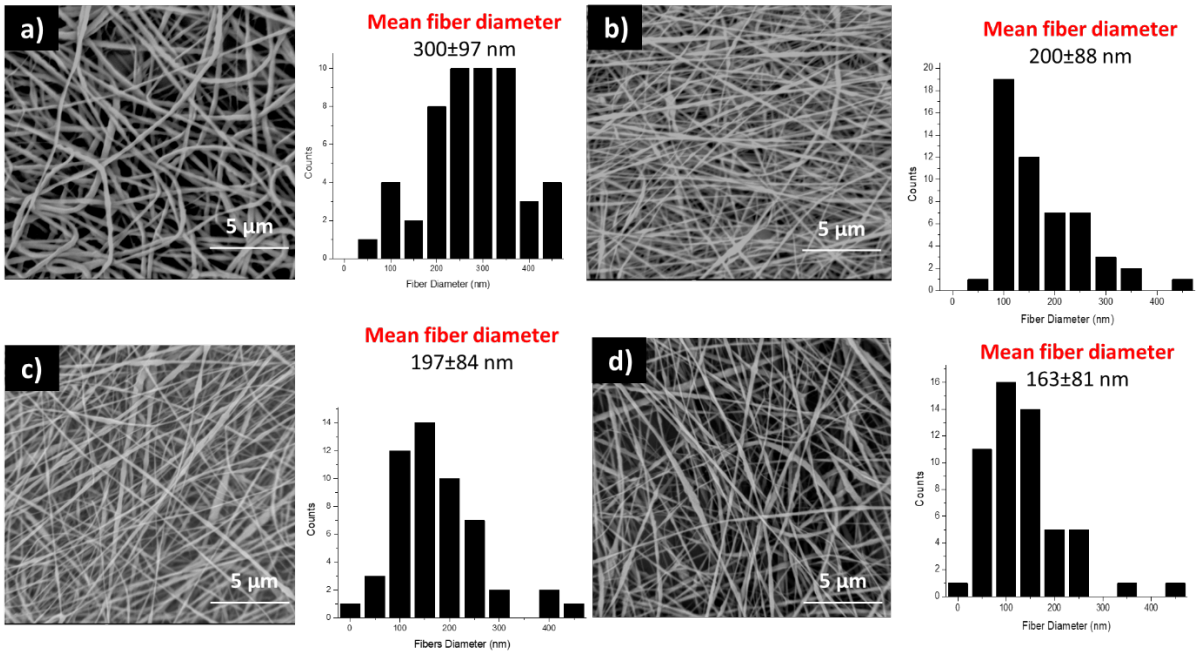

Figure 3: SEM of a) PVDF, b) 1% BN-PVDF, c) 5% BN-PVDF, d) 10% BN-PVDF samples with their fibre distribution bar chart.

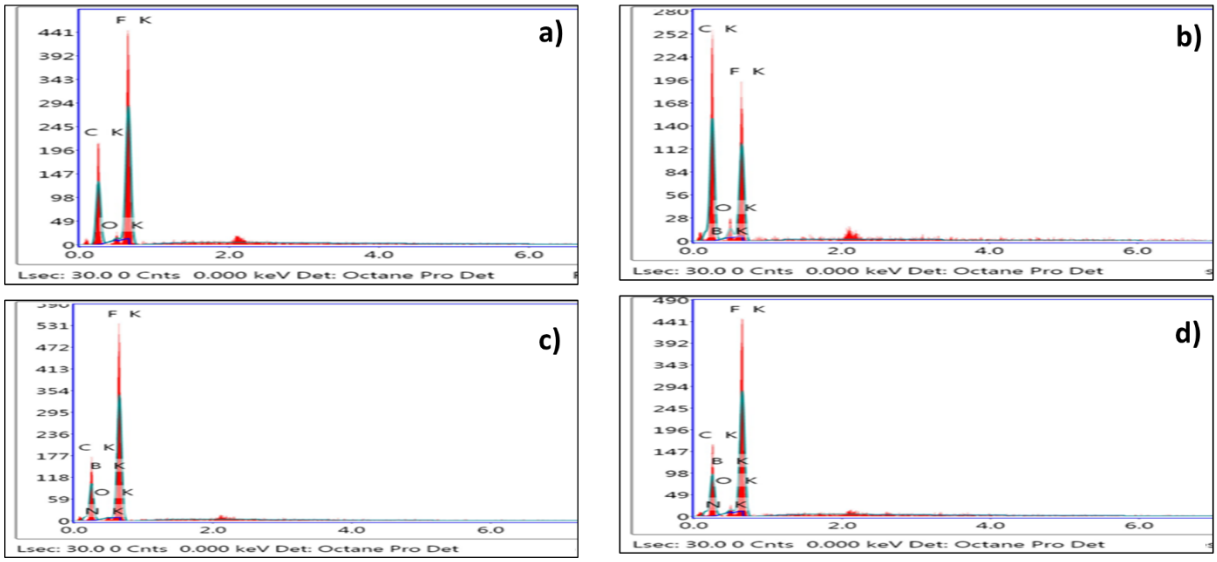

Figure 4: The EDAX of the electrospun mats of a) PVDF, b) 1% BN-PVDF, c) 5% BN-PVDF, d) 10% BN-PVDF samples.

FTIR was used to test the phase of PVDF and hence indicate its piezoelectricity as shown in **Fig. 5(a)** [69, 70]. The samples showed vibrational peaks at 530 cm^{-1} which corresponds to CF_2 bending [71]. All the samples showed β phase exclusive peaks which appear at 445, 473,1431 and 1275 cm^{-1} and also the controversial peak of β phase of at 600 cm^{-1} which indicates the piezoelectric activity of the prepared samples [69]. The common peaks of the β phase with the other phases also appeared in the samples, but all the exclusive peaks of the other phases did not appear in their spectra, indicating that the formed phase is pure β phase. It was found that the intensity of the peaks is inversely related to the F-BNQDs concentration which may be assigned to the interaction between F-BNQDs and the chains of PVDF. Similar results were reported by Kaspar et al. in their study on the effect of carbon flakes on PVDF and also by Rusli et al. in their study on the effect of TiO_2 addition [72, 73].

The results attained from XRD measurements are shown in **Fig. 5(b)**. As observed the β phase peak appeared at 21° which ensures that all the samples are all in the β phase [72]. There are no additional peaks associated with the addition of functionalized BN quantum dots, which may be due to the interactions between F-BNQDs and the chains of PVDF which resulted in the increase in the intensity of the peak of $2\theta = 21^{o}$.

Thermogravimetric analysis was used to inspect the approximate percentage of F-BNQDs in the samples. From **Fig. 5(b)**, it was shown that PVDF showed about 40% mass lost at 470°C and about 88% mass loss at 550 °C. By the addition of 1% F-BNQDs the thermal stability of the PVDF enhanced to be 60% mass loss at about 550 °C. There was a slight

increase in the thermal stability by increasing the BN concentration, which further supports the evidence regarding the interaction between F-BNQDs and PVDF chains.

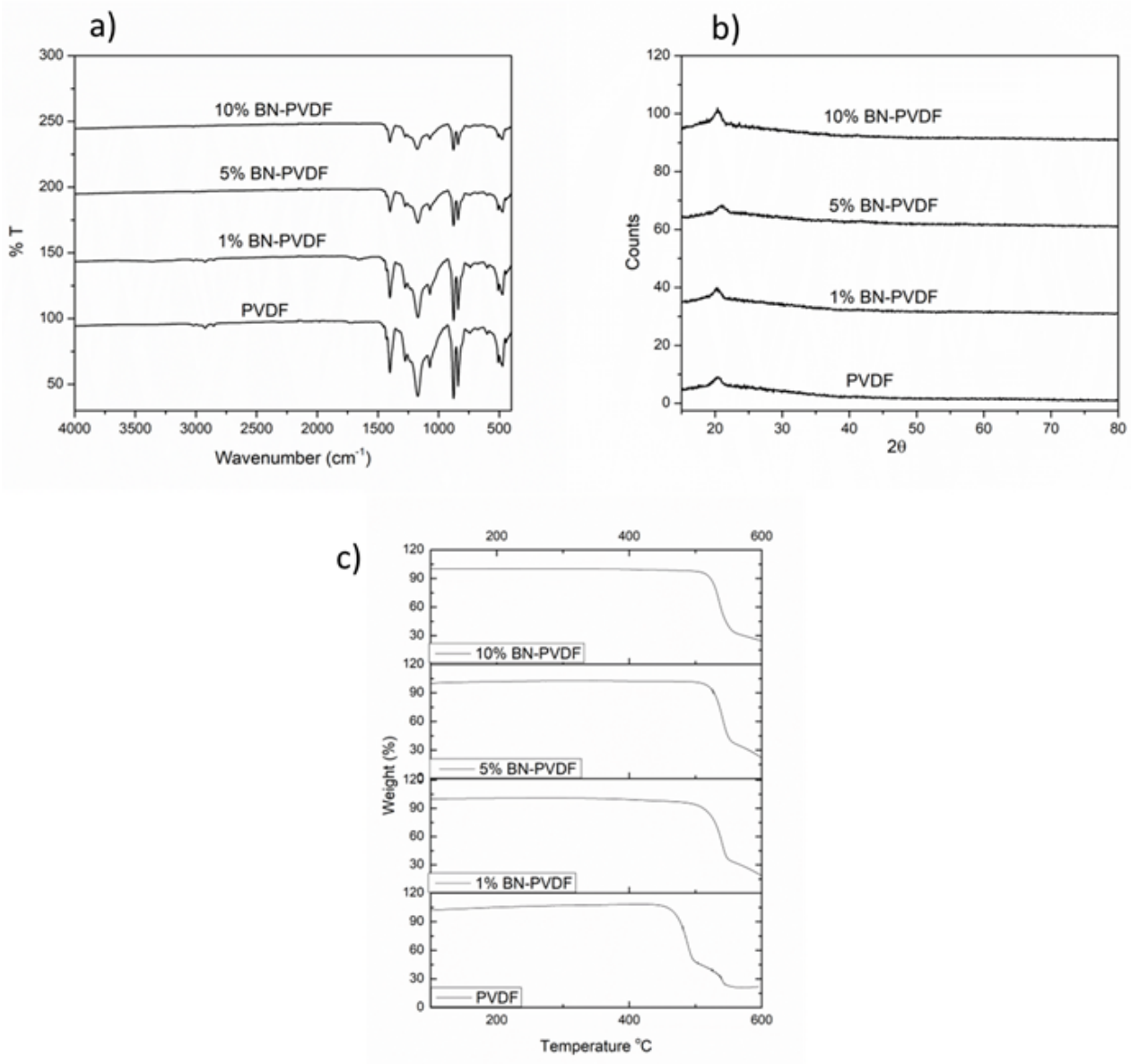

Figure 5: a) FTIR spectra, b) XRD chart and c) TGA measurements of the prepared electrospun samples.

Contact angle measurements were conducted to examine the change in hydrophilicity of the samples. As shown from the results in **Fig. 6(a)**, the increase in F-BNQD concentration enhances the hydrophilicity of the samples. This may be related to the presence of various functional groups due to taurine existence in the F-BNQDs structure. Higher hydrophilicity

generally indicates higher cytocompatibility [74]. The results obtained agree with the results obtained by Qian et al. on the effect of boron nitride addition to polycaprolactone [40]

As displayed in **Fig. 6(b)**, the swelling ratio increases as the functionalized BN concentration increases as there is a relation between swelling (water uptake) and hydrophilicity [51]. **Fig. 6(c)**, shows that the materials degrade gradually, by 5-10% throughout the 28 days. The increased degradation associated with the increase of F-BNQD concentration may be related to the increase in hydrophilicity because of the increase in surface functional groups. Additionally, reducing the diameter of the fiber results in a higher surface area to volume ratio, causing water to penetrate more easily and resulting in faster degradation rates.

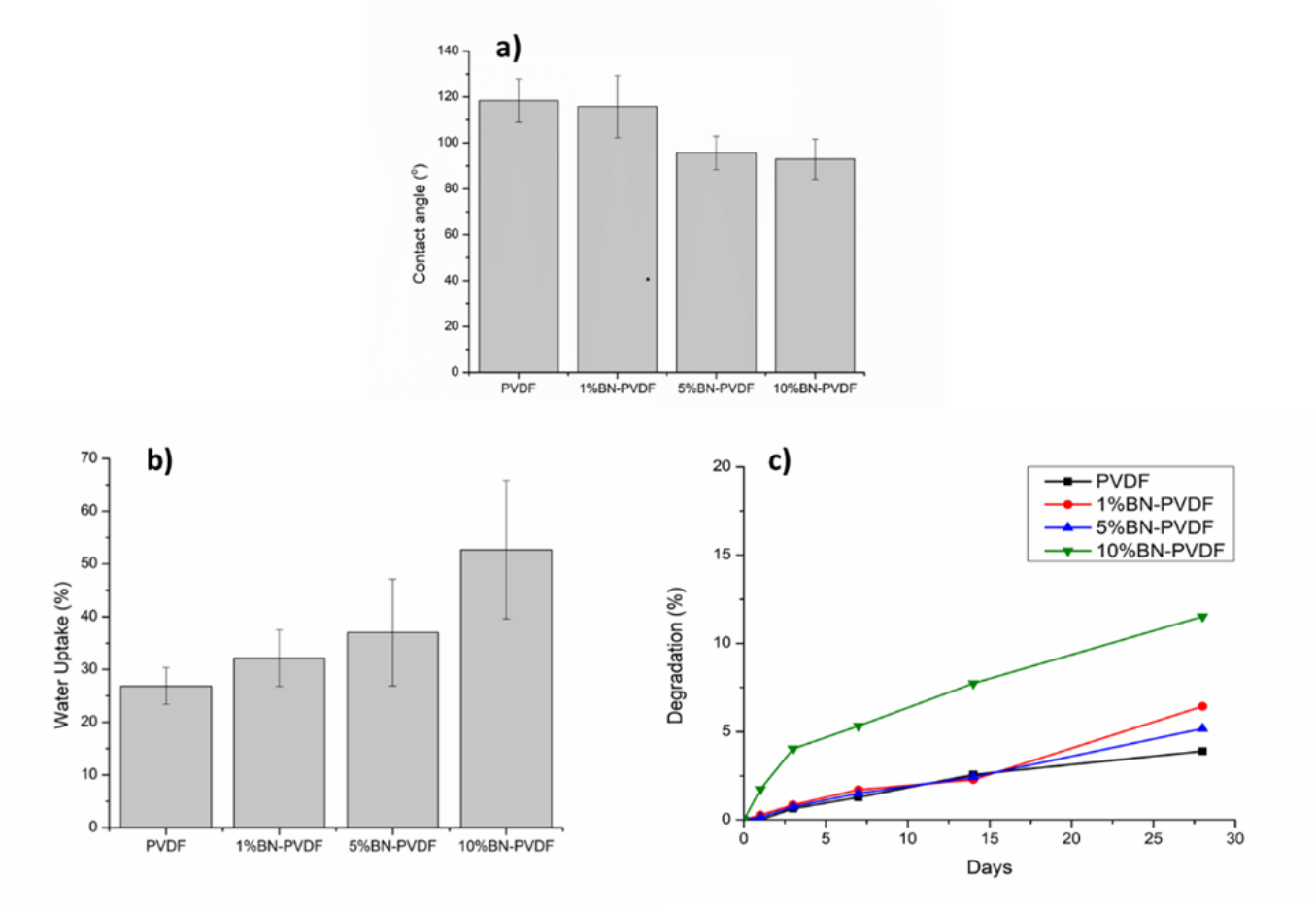

Figure 6: a) Contact angle measurements (n=5), b) water uptake percentage (n=3) and c) degradation properties (n=3) of the prepared samples

Fig. 7 displays the mechanical characteristics of the samples. The PVDF samples showed an average tensile strength of 1.1±0.3 MPa and exhibited a Young's modulus

17.61±5.3 MPa with elongation at break of 31.3±11.3 %. Incorporating 1% F-BNQDs resulted in a an increase in tensile strength to 1.19±0.3 MPa and also an increase in the elongation at break to 43.6±7.1 %, which may be attributed to polymer strengthening and homogenous distribution along the fibres. By increasing the F-BNQD percentage to 5%, there was a slight increase in tensile strength to 1.25±0.5 MPa with a decrease in Young's modulus and also in the elongation at break which may be as a result of the slight stiffness caused by the agglomeration of the F-BNQDs. The mechanical properties of 10% BN-PVDF showed an obvious decrease in mechanical characteristics also due to the agglomeration of the particles.

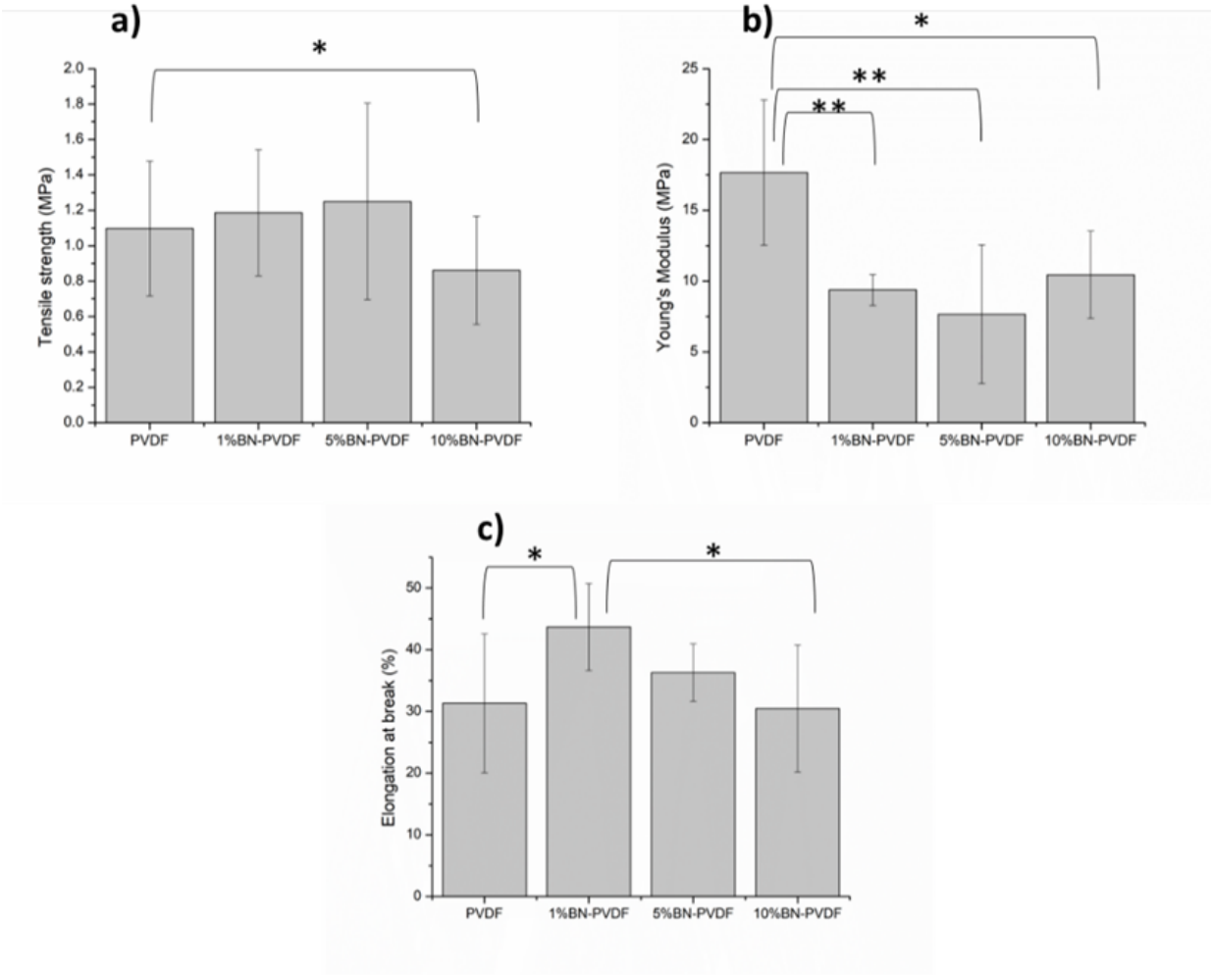

Figure 7: The different mechanical properties of the prepared samples a) Tensile Strength, b) Young's modulus and c) Elongation at break. (n=4) * ($p<0.05$) ** ($p<0.005$)

Schwann cells are glial cells within the peripheral nervous system that have a vital function in aiding the regeneration of neurons, so they were used here to examine the compatibility of the materials for a potential future application in nerve tissue engineering [75]. To examine any possible toxic effect of the samples on Schwann cells we used an LDH assay. As shown from the results in **Fig. 8**, cell death was relatively low in all samples at both 24 and 48h. There was a significant difference between 1% BN-PVDF and 5% BN-PVDF at the 48h time point, with the 1% BN-PVDF showing the highest level of cell death of all samples at ~13% and 5% BN-PVDF exhibiting <2% cell death.

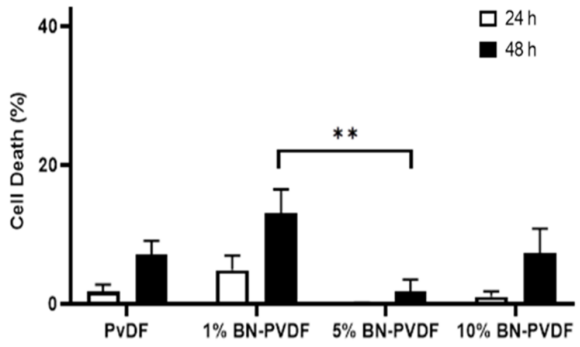

Figure 8: Cytotoxicity in response to the different materials using an assay for lactate dehydrogenase. Data are means ± SEM, n = 3 independent material samples in triplicate. 2-way ANOVA indicated significant effects of time and material, with Tukey's multiple comparisons test used to compare the four materials at each time point (**p<0.005).

As the samples were deemed non-toxic, the ability of the samples to support cell growth *in vitro* was studied. The DAPI stained micrographs showed cells were present on the electrospun nanofibers in all the groups, 48h hours after seeding (**Fig. 9)**.

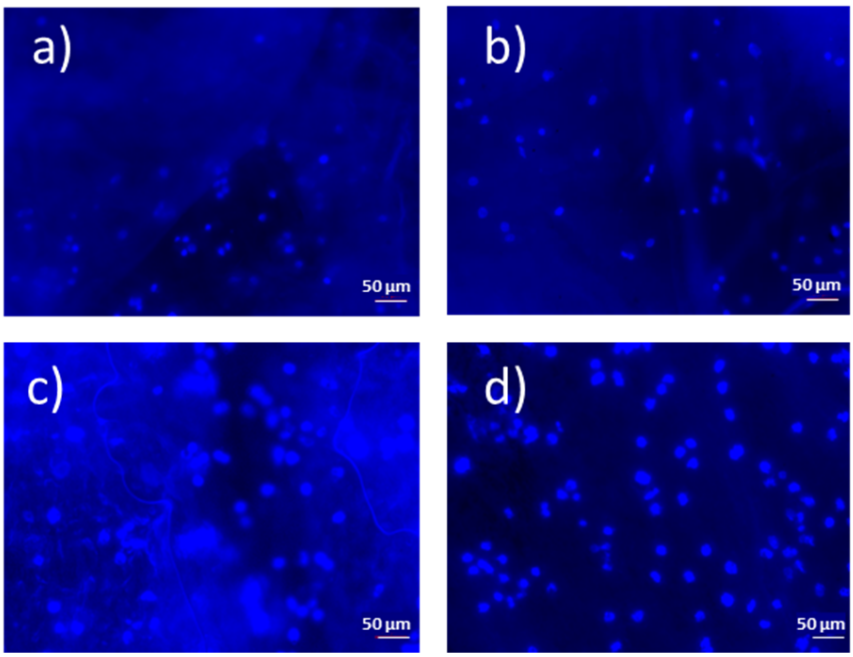

Figure 9: Cells present on the fibres after 48 hours using a cell nuclei stain (DAPI). a) PVDF, b) 1% BN-PVDF, c) 5% BN-PVDF, d) 10% BN-PVDF.

The results are consistent with the LDH assay study findings and indicate the biocompatibility of the materials, indicating that they could be used in further *in vivo* studies. Furthermore, the cell number results are consistent with the trend of the hydrophilicity taken from the water contact angle assay, as cell adhesion is reported to be enhanced through increased hydrophilicity of biomaterials [76, 77]. Cell interaction with the prepared electrospun samples was examined by SEM after 7 days of cell culture as shown in **Fig. 10**. The SEM micrographs give qualitative information about how Schwann cells may behave when grown on the surface of the fibres. As the concentration of F-BNQDs increases within the PVDF fibre mats, the cells exhibit a more spread morphology on the surface of the materials. The spread of Schwann cells over the samples indicates that the cells can grow on the nanofibrous surface confirming its biocompatibility.

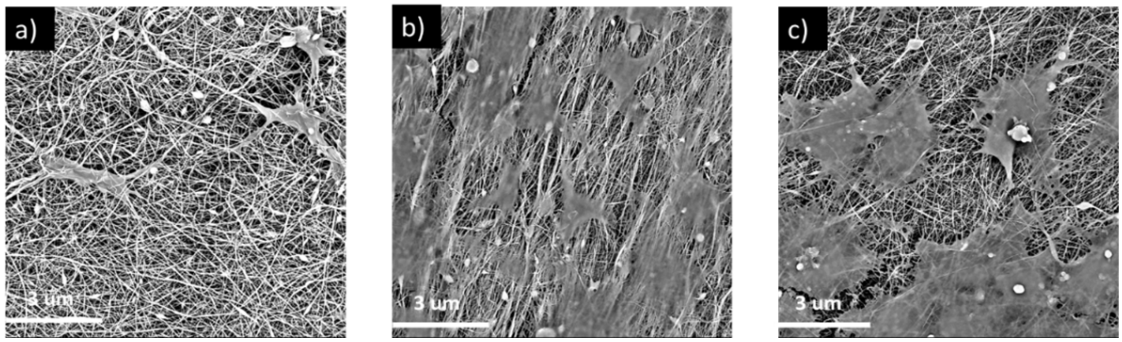

Figure 10: SEM of the Schwann Cells upon the different fibrous mats, imaged 1 week after seeding. a) 1% BN-PVDF, b) 5% BN-PVDF, c) 10% BN-PVDF samples.

Conclusions

The study investigated a green approach for the fabrication of novel functionalized boron nitride quantum dots. F-BNQDs were combined with PVDF in three different concentrations to formulate enhanced nanofibrous biomaterials with the potential for use in neuroregeneration. All the samples were found to have s single β phase indicating high piezoelectric properties. The addition of F-BNQDs to PVDF resulted in altered mechanical properties, enhanced contact angle, degradability, water uptake, and cell attachment. The study concluded that of those options tested, the 5% BN-PVDF showed suitability for further investigation in nerve regeneration applications.

Acknowledgment

The paper is based upon collaborative work between the National Research Centre of Egypt and School of Pharmacy, University College London, UK and supported by UK Academy of Medical Sciences, Daniel Turnberg Fellowship scheme Round 12.

References

1. Gordon T (2020) Peripheral Nerve Regeneration and Muscle Reinnervation. Int J Mol Sci 21:1–24. https://doi.org/10.3390/IJMS21228652
2. Standring S (2022) The History of Nerve Repair. 1–32. https://doi.org/10.1007/978-3-030-21052-6_1
3. Muratori L, Fregnan F, Carta G, Geuna S (2021) Autonomic Nervous System Repair and Regeneration. 1–21. https://doi.org/10.1007/978-3-030-06217-0_2-1
4. Gregory H, Phillips JB (2021) Materials for peripheral nerve repair constructs: Natural proteins or synthetic polymers? Neurochem Int 143:. https://doi.org/10.1016/J.NEUINT.2020.104953

5. Soares RMD, Siqueira NM, Prabhakaram MP, Ramakrishna S (2018) Electrospinning and electrospray of bio-based and natural polymers for biomaterials development. Materials Science and Engineering: C 92:969–982. https://doi.org/10.1016/J.MSEC.2018.08.004
6. Nobile S, Nobile L (2017) Nanotechnology for biomedical applications: Recent advances in neurosciences and bone tissue engineering. Polym Eng Sci 57:644–650. https://doi.org/10.1002/PEN.24595
7. Li X, Zhang Q, Ye D, et al (2017) Fabrication and characterization of electrospun PCL/Antheraea pernyi silk fibroin nanofibrous scaffolds. Polym Eng Sci 57:206–213. https://doi.org/10.1002/PEN.24402
8. Amini S, Saudi A, Amirpour N, et al (2020) Application of electrospun polycaprolactone fibers embedding lignin nanoparticle for peripheral nerve regeneration: In vitro and in vivo study. Int J Biol Macromol 159:154–173. https://doi.org/10.1016/J.IJBIOMAC.2020.05.073
9. Li L, Cook JE, Cheng Z, Zhang X (2017) PVDF/PPy nanofibrous membranes for peripheral nerve lesion treatments. 2017 Joint IEEE International Symposium on Applications of Ferroelectrics, International Workshop on Acoustic Transduction Materials and Devices and Piezoresponse Force Microscopy Workshop, ISAF-IWATMD-PFM 2017 - Conference 48–51. https://doi.org/10.1109/ISAF.2017.8000209
10. Cheng Y, Xu Y, Qian Y, et al (2020) 3D structured self-powered PVDF/PCL scaffolds for peripheral nerve regeneration. Nano Energy 69:104411. https://doi.org/10.1016/J.NANOEN.2019.104411
11. Gryshkov O, Al Halabi F, Kuhn AI, et al (2021) Pvdf and p(Vdf-trfe) electrospun scaffolds for nerve graft engineering: A comparative study on piezoelectric and structural properties, and in vitro biocompatibility. Int J Mol Sci 22:11373. https://doi.org/10.3390/IJMS222111373/S1
12. Ma Y, Wang H, Wang Q, et al (2023) Piezoelectric conduit combined with multi-channel conductive scaffold for peripheral nerve regeneration. Chemical Engineering Journal 452:139424. https://doi.org/10.1016/J.CEJ.2022.139424
13. Lannutti J, Reneker D, Ma T, et al (2007) Electrospinning for tissue engineering scaffolds. Materials Science and Engineering: C 27:504–509. https://doi.org/10.1016/J.MSEC.2006.05.019
14. Ghane N, Khalili S, Nouri Khorasani S, et al (2021) Regeneration of the peripheral nerve via multifunctional electrospun scaffolds. J Biomed Mater Res A 109:437–452. https://doi.org/10.1002/JBM.A.37092
15. Quan Q, Chang B, Meng HY, et al (2016) Use of electrospinning to construct biomaterials for peripheral nerve regeneration. Rev Neurosci 27:761–768. https://doi.org/10.1515/REVNEURO-2016-0032
16. Amr SM, Ekram B (2017) Speculations on the Use of Marine Polysaccharides as Scaffolds for Artificial Nerve 'Side-'Grafts. Biological Activities and Application of Marine Polysaccharides. https://doi.org/10.5772/66460
17. Zhou G, Chen Y, Dai F, Yu X (2023) Chitosan-based nerve guidance conduit with microchannels and nanofibers promotes schwann cells migration and neurite growth. Colloids Surf B Biointerfaces 221:112929. https://doi.org/10.1016/J.COLSURFB.2022.112929

18. Zaszczynska A, Sajkiewicz P, Gradys A (2020) Piezoelectric Scaffolds as Smart Materials for Neural Tissue Engineering. Polymers 2020, Vol 12, Page 161 12:161. https://doi.org/10.3390/POLYM12010161
19. Rahman M, Mahady Dip T, Padhye R, Houshyar S (2023) Review on electrically conductive smart nerve guide conduit for peripheral nerve regeneration. J Biomed Mater Res A 111:1916–1950. https://doi.org/10.1002/JBM.A.37595
20. Kapat K, Shubhra QTH, Zhou M, Leeuwenburgh S (2020) Piezoelectric Nano-Biomaterials for Biomedicine and Tissue Regeneration. Adv Funct Mater 30:1909045. https://doi.org/10.1002/ADFM.201909045
21. Kamel NA (2022) Bio-piezoelectricity: fundamentals and applications in tissue engineering and regenerative medicine. Biophys Rev 14:717. https://doi.org/10.1007/S12551-022-00969-Z
22. Najjari A, Mehdinavaz Aghdam R, Ebrahimi SAS, et al (2022) Smart piezoelectric biomaterials for tissue engineering and regenerative medicine: A review. Biomedizinische Technik 67:71–88. https://doi.org/10.1515/BMT-2021-0265
23. Khang G, Lee SJ, Lee JH, et al (1999) Interaction of fibroblast cells on poly(lactide-co-glycolide) surface with wettability chemogradient. Biomed Mater Eng 9:179–187
24. Sasabe H, Saito S, Asahina M, Kakutani H (1969) Dielectric relaxations in poly(vinylidene fluoride). Journal of Polymer Science Part A-2: Polymer Physics 7:1405–1414. https://doi.org/10.1002/POL.1969.160070810
25. Mokhtari F, Shamshirsaz M, Latifi M (2016) Investigation of β phase formation in piezoelectric response of electrospun polyvinylidene fluoride nanofibers: LiCl additive and increasing fibers tension. Polym Eng Sci 56:61–70. https://doi.org/10.1002/PEN.24192
26. Liang J, Zeng H, Qiao L, et al (2022) 3D Printed Piezoelectric Wound Dressing with Dual Piezoelectric Response Models for Scar-Prevention Wound Healing. ACS Appl Mater Interfaces 14:30507–30522. https://doi.org/10.1021/ACSAMI.2C04168/SUPPL_FILE/AM2C04168_SI_001.PDF
27. Kao FC, Ho HH, Chiu PY, et al (2022) Self-assisted wound healing using piezoelectric and triboelectric nanogenerators. http://www.tandfonline.com/action/journalInformation?show=aimsScope&journalCode=tsta20#VmBmuzZFCUk 23:1–16. https://doi.org/10.1080/14686996.2021.2015249
28. Trueman RP, Ahlawat AS, Phillips JB (2022) A Shock to the (Nervous) System: Bioelectricity Within Peripheral Nerve Tissue Engineering. Tissue Eng Part B Rev 28:1137–1150. https://doi.org/10.1089/TEN.TEB.2021.0159
29. Mao R, Yu B, Cui J, et al (2022) Piezoelectric stimulation from electrospun composite nanofibers for rapid peripheral nerve regeneration. Nano Energy 98:107322. https://doi.org/10.1016/J.NANOEN.2022.107322
30. Zhang J, Wang H, Blanloeuil P, et al (2020) Enhancing the triboelectricity of stretchable electrospun piezoelectric polyvinylidene fluoride/boron nitride nanosheets composite nanofibers. Composites Communications 22:100535. https://doi.org/10.1016/J.COCO.2020.100535
31. Torres-Giner S, Pérez-Masiá R, Lagaron JM (2016) A review on electrospun polymer nanostructures as advanced bioactive platforms. Polym Eng Sci 56:500–527. https://doi.org/10.1002/PEN.24274

32. Ruan L, Yao X, Chang Y, et al (2018) Properties and Applications of the β Phase Poly(vinylidene fluoride). Polymers (Basel) 10:. https://doi.org/10.3390/POLYM10030228
33. Ge X, Wu S, Shen W, et al (2022) Preparation of Polyvinylidene Fluoride–Gold Nanoparticles Electrospinning Nanofiber Membranes. Bioengineering 9:. https://doi.org/10.3390/bioengineering9040130
34. Cheng Y, Xu Y, Qian Y, et al (2020) 3D structured self-powered PVDF/PCL scaffolds for peripheral nerve regeneration. Nano Energy 69:104411. https://doi.org/10.1016/J.NANOEN.2019.104411
35. Gryshkov O, Al Halabi F, Kuhn AI, et al (2021) Pvdf and p(Vdf-trfe) electrospun scaffolds for nerve graft engineering: A comparative study on piezoelectric and structural properties, and in vitro biocompatibility. Int J Mol Sci 22:11373. https://doi.org/10.3390/IJMS222111373/S1
36. Abzan N, Kharaziha M, Labbaf S (2019) Development of three-dimensional piezoelectric polyvinylidene fluoride-graphene oxide scaffold by non-solvent induced phase separation method for nerve tissue engineering. Mater Des 167:. https://doi.org/10.1016/j.matdes.2019.107636
37. Merlo A, Mokkapati VRSS, Pandit S, Mijakovic I (2018) Boron nitride nanomaterials: biocompatibility and bio-applications. Biomater Sci 6:2298–2311. https://doi.org/10.1039/C8BM00516H
38. Li H, Tay RY, Tsang SH, et al (2015) Controllable Synthesis of Highly Luminescent Boron Nitride Quantum Dots. Small 11:6491–6499. https://doi.org/10.1002/SMLL.201501632
39. Farshid B, Lalwani G, Shir Mohammadi M, et al (2017) Boron nitride nanotubes and nanoplatelets as reinforcing agents of polymeric matrices for bone tissue engineering. J Biomed Mater Res B Appl Biomater 105:406–419. https://doi.org/10.1002/JBM.B.33565
40. Qian Y, Xu Y, Yan Z, et al (2021) Boron nitride nanosheets functionalized channel scaffold favors microenvironment rebalance cocktail therapy for piezocatalytic neuronal repair. Nano Energy 83:. https://doi.org/10.1016/j.nanoen.2021.105779
41. Yukawa H, Sato K, Baba Y (2023) Theranostics applications of quantum dots in regenerative medicine, cancer medicine, and infectious diseases. Adv Drug Deliv Rev 200
42. Zeng Z, Yu D, He Z, et al (2016) Graphene Oxide Quantum Dots Covalently Functionalized PVDF Membrane with Significantly-Enhanced Bactericidal and Antibiofouling Performances. Sci Rep 6:. https://doi.org/10.1038/srep20142
43. Jakaria M, Azam S, Haque ME, et al (2019) Taurine and its analogs in neurological disorders: Focus on therapeutic potential and molecular mechanisms. Redox Biol 24:. https://doi.org/10.1016/J.REDOX.2019.101223
44. Jang HC, Lee S, Choi SL, et al (2017) Taurine directly binds to oligomeric amyloid-β and recovers cognitive deficits in Alzheimer model mice. Adv Exp Med Biol 975:233–241. https://doi.org/10.1007/978-94-024-1079-2_21/FIGURES/2
45. Che Y, Hou L, Sun F, et al (2018) Taurine protects dopaminergic neurons in a mouse Parkinson's disease model through inhibition of microglial M1 polarization. Cell Death Dis 9:. https://doi.org/10.1038/S41419-018-0468-2
46. Li K, Shi X, Luo M, et al (2019) Taurine protects against myelin damage of sciatic nerve in diabetic peripheral neuropathy rats by controlling apoptosis of schwann cells via

NGF/Akt/GSK3β pathway. Exp Cell Res 383:. https://doi.org/10.1016/J.YEXCR.2019.111557
47. Hernández-Benítez R, Ramos-Mandujano G, Pasantes-Morales H (2012) Taurine stimulates proliferation and promotes neurogenesis of mouse adult cultured neural stem/progenitor cells. Stem Cell Res 9:24–34. https://doi.org/10.1016/J.SCR.2012.02.004
48. Jerome R, Sundramoorthy AK (2019) Hydrothermal Synthesis of Boron Nitride Quantum Dots/Poly(Luminol) Nanocomposite for Selective Detection of Ascorbic Acid. J Electrochem Soc 166:B3017–B3024. https://doi.org/10.1149/2.0041909JES/XML
49. Gee S, Johnson B, Smith AL (2018) Optimizing electrospinning parameters for piezoelectric PVDF nanofiber membranes. J Memb Sci 563:804–812. https://doi.org/10.1016/J.MEMSCI.2018.06.050
50. Schneider CA, Rasband WS, Eliceiri KW (2012) NIH Image to ImageJ: 25 years of Image Analysis. Nat Methods 9:671. https://doi.org/10.1038/NMETH.2089
51. Kandil H, Ekram B, Abo-Zeid MAM (2022) Cytocompatibility of MG-63 osteosarcoma cells on chitosan/hydroxyapatite/lignin hybrid composite scaffold in vitro. Biomedical Materials 18:015002. https://doi.org/10.1088/1748-605X/AC9F92
52. Deyab NM, Ekram B, Badr KR, et al (2022) Antiviral Electrospun Polyamide Three-Layered Mask Filter Containing Metal Oxide Nanoparticles and Black Seed Oil. ACS Omega 7:44438–44447. https://doi.org/10.1021/ACSOMEGA.2C06611/ASSET/IMAGES/LARGE/AO2C06611_0008.JPEG
53. El-Gendy DM, Abdel Ghany NA, Allam NK (2019) Green, single-pot synthesis of functionalized Na/N/P co-doped graphene nanosheets for high-performance supercapacitors. Journal of Electroanalytical Chemistry 837:30–38. https://doi.org/10.1016/J.JELECHEM.2019.02.009
54. Angizi S, Hatamie A, Ghanbari H, Simchi A (2018) Mechanochemical Green Synthesis of Exfoliated Edge-Functionalized Boron Nitride Quantum Dots: Application to Vitamin C Sensing through Hybridization with Gold Electrodes. ACS Appl Mater Interfaces 10:28819–28827. https://doi.org/10.1021/ACSAMI.8B07332/SUPPL_FILE/AM8B07332_SI_001.PDF
55. Liu B, Yan S, Song Z, et al (2016) One-Step Synthesis of Boron Nitride Quantum Dots: Simple Chemistry Meets Delicate Nanotechnology. Chemistry – A European Journal 22:18899–18907. https://doi.org/10.1002/CHEM.201603935
56. El-Gendy DM, Afifi IM, Allam NK (2019) Eco-friendly, one-step synthesis of cobalt sulfide-decorated functionalized graphene for high-performance supercapacitors. J Energy Storage 24:100760. https://doi.org/10.1016/J.EST.2019.100760
57. Shakir I, Shahid M, Yang HW, Kang DJ (2010) Structural and electrochemical characterization of α-MoO3 nanorod-based electrochemical energy storage devices. Electrochim Acta 56:376–380. https://doi.org/10.1016/J.ELECTACTA.2010.09.028
58. Bleda-Martínez MJ, Lozano-Castelló D, Morallón E, et al (2006) Chemical and electrochemical characterization of porous carbon materials. Carbon N Y 44:2642–2651. https://doi.org/10.1016/J.CARBON.2006.04.017
59. Li H, Tay RY, Tsang SH, et al (2015) Controllable Synthesis of Highly Luminescent Boron Nitride Quantum Dots. Small 11:6491–6499. https://doi.org/10.1002/SMLL.201501632

60. Lin L, Xu Y, Zhang S, et al (2014) Fabrication and Luminescence of Monolayered Boron Nitride Quantum Dots. Small 10:60–65. https://doi.org/10.1002/SMLL.201301001
61. Lei Z, Xu S, Wan J, Wu P (2015) Facile preparation and multifunctional applications of boron nitride quantum dots. Nanoscale 7:18902–18907. https://doi.org/10.1039/C5NR05960G
62. Xue Q, Zhang H, Zhu M, et al (2016) Hydrothermal synthesis of blue-fluorescent monolayer BN and BCNO quantum dots for bio-imaging probes. RSC Adv 6:79090–79094. https://doi.org/10.1039/C6RA16744F
63. Huo B, Liu B, Chen T, et al (2017) One-step synthesis of fluorescent boron nitride quantum dots via a hydrothermal strategy using melamine as nitrogen source for the detection of ferric ions. Langmuir 33:10673–10678. https://doi.org/10.1021/ACS.LANGMUIR.7B01699/SUPPL_FILE/LA7B01699_SI_001.PDF
64. Tanvir Hasan M, Gonzalez-Rodriguez R, Ryan C, et al (2018) Photo-and Electroluminescence from Nitrogen-Doped and Nitrogen–Sulfur Codoped Graphene Quantum Dots. Adv Funct Mater 28:1804337. https://doi.org/10.1002/ADFM.201804337
65. Bao L, Zhang ZL, Tian ZQ, et al (2011) Electrochemical Tuning of Luminescent Carbon Nanodots: From Preparation to Luminescence Mechanism. Advanced Materials 23:5801–5806. https://doi.org/10.1002/ADMA.201102866
66. Gan Z, Xu H, Hao Y (2016) Mechanism for excitation-dependent photoluminescence from graphene quantum dots and other graphene oxide derivates: consensus, debates and challenges. Nanoscale 8:7794–7807. https://doi.org/10.1039/C6NR00605A
67. Ray M, Basu TS, Jana A, et al (2010) Luminescent core-shell nanostructures of silicon and silicon oxide: Nanodots and nanorods. J Appl Phys 107:064311. https://doi.org/10.1063/1.3330658
68. Xue Y, Hu X (2020) Electrospun Silk-Boron Nitride Nanofibers with Tunable Structure and Properties. Polymers (Basel) 12:. https://doi.org/10.3390/POLYM12051093
69. Cai X, Lei T, Sun D, Lin L (2017) A critical analysis of the α, β and γ phases in poly(vinylidene fluoride) using FTIR. RSC Adv 7:15382–15389. https://doi.org/10.1039/C7RA01267E
70. Mireja S, Khakhar D V. (2023) Methods to characterize the crystal polymorphs of polyvinylidene fluoride using Fourier transform infrared spectroscopy. Polym Eng Sci 63:2857–2870. https://doi.org/10.1002/PEN.26410
71. Salimi A, Yousefi AA (2003) FTIR studies of β-phase crystal formation in stretched PVDF films. Polym Test 22:699–704. https://doi.org/10.1016/S0142-9418(03)00003-5
72. Kaspar P, Sobola D, Částková K, et al (2020) Characterization of polyvinylidene fluoride (Pvdf) electrospun fibers doped by carbon flakes. Polymers (Basel) 12:1–15. https://doi.org/10.3390/polym12122766
73. Rusli UN, Alias NH, Shahruddin MZ, Othman NH (2016) Photocatalytic Degradation of Oil using Polyvinylidene Fluoride/Titanium Dioxide Composite Membrane for Oily Wastewater Treatment. MATEC Web of Conferences 69:05003. https://doi.org/10.1051/MATECCONF/20166905003
74. Ekram B, Abd El-Hady BM, El-Kady AM, et al (2019) Enhancing the Stability, Hydrophilicity, Mechanical and Biological Properties of Electrospun Polycaprolactone

in Formic Acid/Acetic Acid Solvent System. Fibers and Polymers 20:715–724. https://doi.org/10.1007/s12221-019-8795-1
75. Bolaina-Lorenzo E, Martinez-Ramos C, Monleón-Pradas M, et al (2016) Electrospun polycaprolactone/chitosan scaffolds for nerve tissue engineering: physicochemical characterization and Schwann cell biocompatibility. Biomedical Materials 12:015008. https://doi.org/10.1088/1748-605X/12/1/015008
76. Horbett TA, Waldburger JJ, Ratner BD, Hoffman AS (1988) Cell adhesion to a series of hydrophilic-hydrophobic copolymers studied with a spinning disc apparatus. J Biomed Mater Res 22:383–404. https://doi.org/10.1002/JBM.820220503
77. Ekram B, Abd El-Hady BM, El-Kady AM, et al (2021) Enhanced mesenchymal stem cells growth on antibacterial microgrooved electrospun zinc chloride/polycaprolactone conduits for peripheral nerve regeneration. J Bioact Compat Polym. https://doi.org/10.1177/0883911520988305